Stellar Population Synthesis
–
Basic Methodology and Examples on Star Formation Rate and Metallicity

Steffen Silies
Email: steffen.silies@uni-bielefeld.de

20.08.2018

Contents

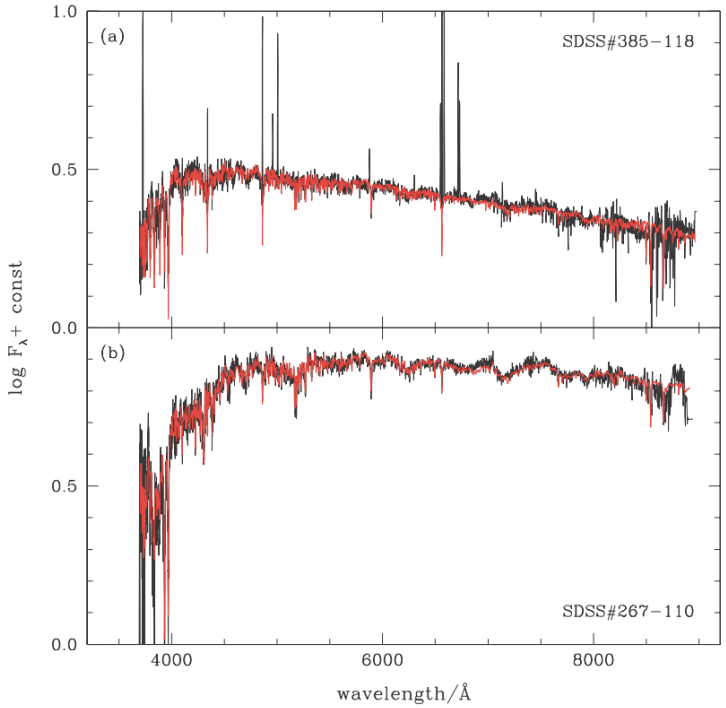

Fig. 1: Model SEDs (red) from (Bruzual and Charlot, 2003) for measured data (black) from the Sloan Digital Sky Survey

1 Galactic Spectral Energy Distributions

When galaxies outside of the Milky Way are observed, for most of them, individual stars cannot be resolved. The radiation arriving at the telescope is combined from all the galaxies' constituents, yet astronomers aim to gain insight about the components, disentangled from each other. One possible approach to do so is to examine the spectral energy distribution (SED) of the incoming light. Examples of such distributions can be seen in Fig. 1 (the black graphs).

The SED summarises which wavelength contributes how large a fraction of the radiation's energy. It contains information about the galaxies' constituents in the form of emission and absorption lines as well as the smoother, more general shape. To extract this information, one option is a simulation of SEDs for theoretical galaxies of various ages and constitutions. From a catalogue of simulated data, a best match may be determined – suggesting that the observed galaxy should resemble this simulated one. The technique of stellar population synthesis (SPS) follows this approach.

2 Stellar Population Synthesis

In (Conroy, 2013), the general process of stellar population synthesis is outlined. As mentioned in the introduction, SPS is a technique that provides physically plausible models of galactic spectral energy distributions and allows to fit data from observations to these models to deduce estimates of the observed galaxies' properties. The properties this review focuses on are *star formation rate* (SFR) and *metallicity* (often abbreviated Z, as in formulae). Other properties of interest may include mass-to-light ratios or dust mass and distribution.

The basic idea of SPS is to "synthesise" a model galaxy's SED from the radiative contributions of its constituents. The most important contributions are those of the stars, beyond that, most models also consider contributions from dust. (Conroy, 2013) criticises that most of the SPS routines in wide use lack consideration of nebular emission. The basic building blocks of the synthesis are *simple stellar populations* (SSPs), groups of stars that originate at the same time with the same metallicity. The final synthesized model is called a *composite stellar population* (CSP), its SED is the model data can be fit to. The process is illustrated in Fig. 2.

2.1 Simple Stellar Populations

A number of stars produced at the same point in time are called *coeval*. A coeval group of stars at a uniform starting metallicity (in the context of SPS: a simple stellar population) occupies a track in the colour-magnitude diagram (CMD), stars of different mass lying at different positions within the track. How many stars a newly created population contains at each mass is expressed with the *initial mass function* (IMF). Thus, for a certain IMF, that may be given by theoretic considerations, further calculations yield the track occupied by the population in the CMD at any desired time.

The positions in the CMD can then be used to deduce effective temperatures T_{eff} and surface gravity g of the stars. From libraries of stellar spectra, the radiative contribution of the stars, according to their spectral type and luminosity class is determined. All the contributions are summed up to yield a total for the population, $f_{\text{SSP}}(t, Z)$, a spectral energy density dependent on the metallicity the stars originated at and the time of the observation. This summing is typically done in a way that can be expressed as an integration:

$$f_{\text{SSP}}(t, Z) = \int_{m_1}^{m_2} \mathrm{d}M \, \Phi(M) \, f_{\text{star}}(T_{\text{eff}}(M), \log g(M);\, t, Z) \quad ,$$

where $\Phi(M)$ is the IMF and the integration is carried out along zero-age main sequence masses M. The lower mass limit is given by the mass required

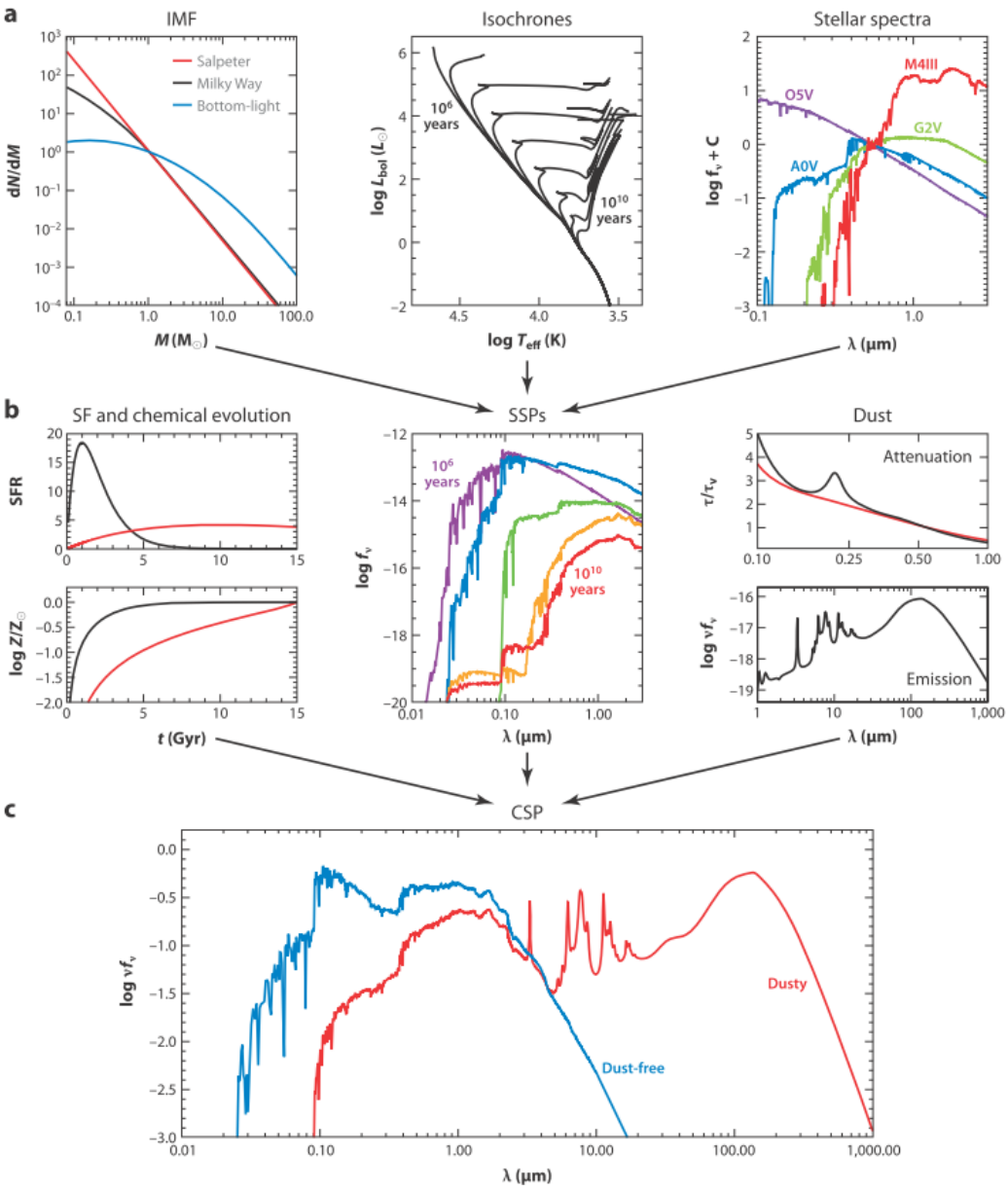

Fig. 2: A schematic from (Conroy, 2013) that visualises the process of SPS. The simple stellar populations in the middle, computed from the information of the top row, get combined into the composite ones, the final SEDs of which are indicated at the bottom.

to start hydrogen burning, the upper one depends on the stellar evolution theories employed.

2.2 Composite Stellar Populations

The SSPs each merely describe one group of stars formed at one point in time with one uniform metallicity. To simulate a galaxy, a whole star formation history (SFH) needs to be considered. Furthermore, formation might occur at various metallicities, though this fact is often simplified to a single Z for all star formation in the model galaxy. Thus, to form a CSP, another integration is carried out along formation ages t' and metallicities Z:

$$f_{\mathrm{CSP}}(t) = \int_0^t \mathrm{d}t' \int_0^{Z_{\max}} \mathrm{d}Z \left(\mathrm{SFR}(t-t') P(Z, t-t') f_{\mathrm{SSP}}(t, Z) e^{-\tau_d(t')} + A f_{\mathrm{dust}}(t', Z) \right) \quad ,$$

where P is the probability density in Z (reduced to a delta peak in the case of a single formation metallicity) and additional terms treating dust appear, τ_d being the optical depth for dust absorption, the $A f_{\mathrm{dust}}(t', Z)$ term adding dust emission. In this way, chemical evolution and dust contributions enter the simulated SED, as Fig. 2 indicates. SFR is often modeled as exponentially declining, possibly with a period of increasing SFR at the beginning of the galaxy's lifetime.

2.3 Fitting the Completed Model

A CSP is a physically plausible model of a galaxy and provides an SED that represents the measurement results expected from a galaxy with its properties. To find a matching model for actual measurements, a fit is carried out – but usually in SPS, fitting parameters are not the galactic properties! Instead, the typical routine is as follows: For the entire "phase space" of plausible galactic property combinations, a "grid" of CSPs is created, containing, for example, 100 000 possible models, as in (Salim et al., 2007). Every model is then compared to every measurement and in this comparison, additional parameters appear that tune the model to mimic the measured SED as closely as possible. These additional parameters are the ones being fit, in most cases with a χ^2-minimising approach.

Comparisons are carried out at specially picked points in the SED, at emission or absorption lines or using photometric indices. The χ^2-type sum of squared residuals between model and data at these points is the quantity minimised in the fit. Thus, not the entire shape of the SED is necessarily imitated, though results can look quite convincing, as seen in Fig. 1. Aside from reducing demands on computing power, the selection of a few points

of comparison can also help to avoid problems with features known to be ambiguous as to their origin. Such ambiguous features can for example arise either from an increase in a galaxy's age or metallicity, with no way to decide which one the real cause is.

3 Results on Star Formation

The publications of (Salim et al., 2007) and (da Cunha et al., 2010) are selected to provide examples of the application of SPS to study star formation rates in galaxies. (Salim et al., 2007) is treated in a bit more detail, to illustrate the SPS process, while from (da Cunha et al., 2010), only the most remarkable result is described.

3.1 SFR in the Local Universe and Active Galactic Nuclei (Salim et al., 2007)

Considering a large sample of about 50 000 galaxies in the local universe (as determined by redshift, $z \approx 0.1$), Samir Salim and colleagues combine data from the GALEX UV telescope and the SDSS (Sloan Digital Sky Survey) for their stellar population synthesis investigation. They thus cover a wide spectral region, reaching from near-infrared (i and z bands) to GALEX' UV measurements (filters at 1528 Å and 2271 Å) and want to compare their method of SFR estimation with ones that utilise the Hα line.

For further analysis, diagnostics based on Hydrogen, Oxygen and Nitrogen emission lines are employed to split the sample into groups with common attributes. There are two groups classified as "star forming", one for high and one for lower signal-to-noise ratio (S/N), a group with strong radiation attributed to an active galactic nucleus (AGN), a composite group that exhibits star forming as well as AGN characteristics, and a group for galaxies that lack any Hα emission.

3.1.1 Method

With the SPS code from (Bruzual and Charlot, 2003), the authors create 10^5 galaxy models and compare the observed SEDs to these models. The comparison uses the flux at the seven SDSS and GALEX photometric indices, dubbed $F_{\mathrm{obs},X}$ for the observations and $F_{\mathrm{mod},X}$ for the models, X denoting the photometric band. For a given observation, model comparisons are labelled with counting index i and for each comparison, an optimal scaling factor a_i is

fit, minimising the expression:

$$\chi_i^2 = \sum_X \left[\frac{F_{\mathrm{obs},X} - a_i \, F_{\mathrm{mod},X}}{\sigma(F_{\mathrm{obs},X})} \right]^2 \quad ,$$

where the sigma indicates observational error. These χ_i^2 are then used to assign a weight $w_i = \exp(-\chi_i^2/2)$ to the comparison, and the weights of all the comparisons form a PDF, a probability density function of the models for that observation.

Every model carries its set of galactic properties, including the star formation rate. The authors' final estimate of a property is the average computed from an observation's PDF of comparisons. They retain the entire PDFs, however, and also report formal errors to their estimates as 1/4 of the PDF's 2.5-97.5 percentile range. Note that these density functions need by no means be Gaussian, hence the term "formal" error. In a Gaussian distribution, 1/4 of that percentile range would correspond to 1σ.

3.1.2 Results

To gain insight about the validity of their method, Salim et al. compared SFR results to those of a 2004 study that relied on Hα emission for its estimates. Some of these comparisons are shown in Fig. 3: If restricted to star forming galaxies that exhibit high S/N and lack an AGN, both methods compare very well (graph on the right), for the other galaxy groups, though, there is not quite as much agreement (graphs on the left). In the case of the ones lacking Hα emission, it is only natural that the Hα-method yields no valid results. The galaxies with high AGN contributions, however, also show low sensitivity of the Hα-method over a vast range of variation in SFR as estimated by Salim et al. The latter fact serves as one of the reasons why the authors suggest their method as a useful alternative for galaxies with strong AGN.

The study's main results are the estimates of SFR for the observed galaxies, these are collected in Fig. 4. Shown are greyscale heatmaps of the galaxy number density in bins that represent a combination of a galaxy's stellar mass content $M_\star$ and the *specific star formation rate*, i. e. SFR divided by $M_\star$. All graphs are supplemented by a dashed line indicating a constant SFR of $1 M_\odot \mathrm{yr}^{-1}$, which in the specific SFR presentation naturally slants downward for higher $M_\star$. The units of $M_\star$ used are solar masses, so for example the 11 in the logarithmic mass axis corresponds to $1 \times 10^{11} M_\odot$.

The most straightforward diagram, the one on the upper left of the figure, simply shows the distribution of all observed galaxies in the $M_\star$-SFR/$M_\star$ plane. Most galaxies seem to concentrate between about 10 and 11 solar

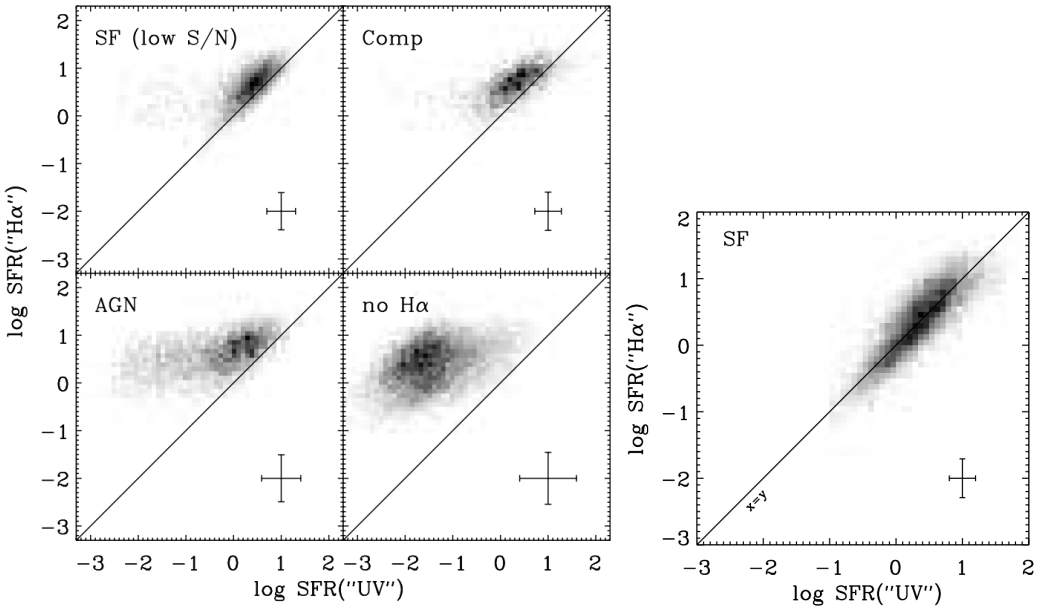

Fig. 3: Comparisons of SFR estimates from (Salim et al., 2007) and a study by Brinchmann et al. from 2004 that used Hα emission. Brightness indicates the number of galaxies in the diagrams' bins.

masses at SFR just above a solar mass per year. From this most populated region, though, a tail extends downward to lower SFR as well. The graphs on the right that separate the various galaxy groups seem to suggest that the main "pile" consists mostly of star forming galaxies, while the tail is made up of those with no Hα emission. The galaxies with AGN seem to fall in between.

These trends find confirmation in the diagrams at the bottom of the figure, these do not assign equal weight to every observed galaxy but rather weight them by the volume they occupy within the observed region, after various corrections. The authors' interpretation of these findings is that of a "star forming sequence", extending up to about $2 \times 10^{11} M_{\odot}$, and a separate population of quiescent galaxies at high masses with much lower SFR. They then argue that galaxies with strong AGN emission continue the star forming sequence, providing a kind of "bridge" to the high-mass quiescent galaxies. This notion is supported by Fig. 5, in which they once again show populations in the $M_{\star}$-SFR/$M_{\star}$ plane, this time concentrating only on the star forming galaxies, the ones that show characteristics of star forming as well as AGN and the ones dominated by AGN emission.

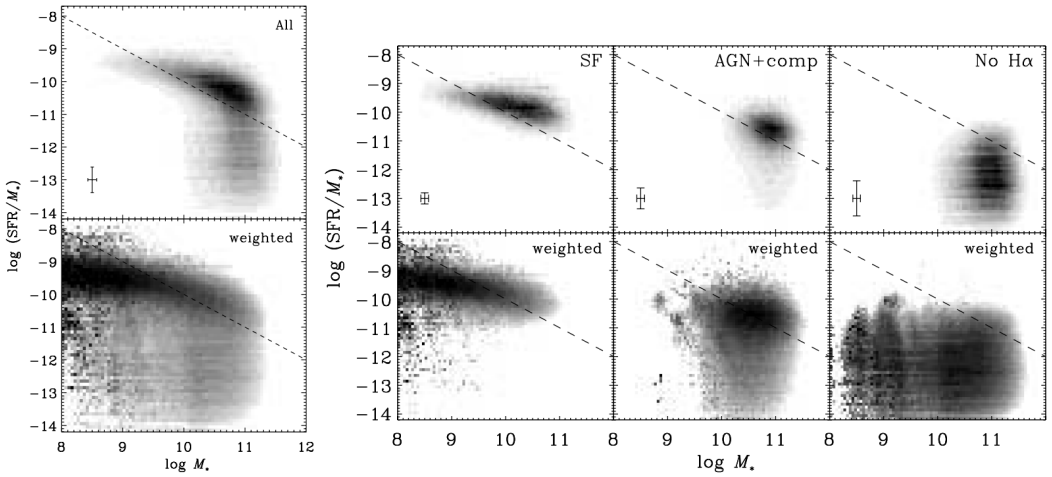

Fig. 4: Results for specific SFR from Salim et al. Brightness indicates bin population, the dashed line in each graph traces a constant SFR of a solar mass per year. While in the graphs at the top, every galaxy is assigned equal weight, the bottom ones are weighted according to the "volume in which a galaxy would be visible taking into account redshift and apparent magnitude limits, and the solid angle of a survey" (Salim et al., 2007)
. In the volume-corrected graphs, the grey shades indicate the number density logarithmically, across 2 orders of magnitude.

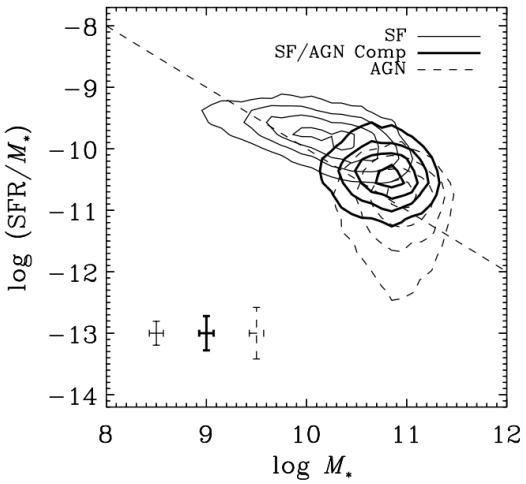

Fig. 5: Specific SFR vs. $M_\star$ for star forming, AGN-dominated and composite galaxies from (Salim et al., 2007). The series of contours enclose the 10th, 30th, 50th and 70th percentiles of the PDFs.

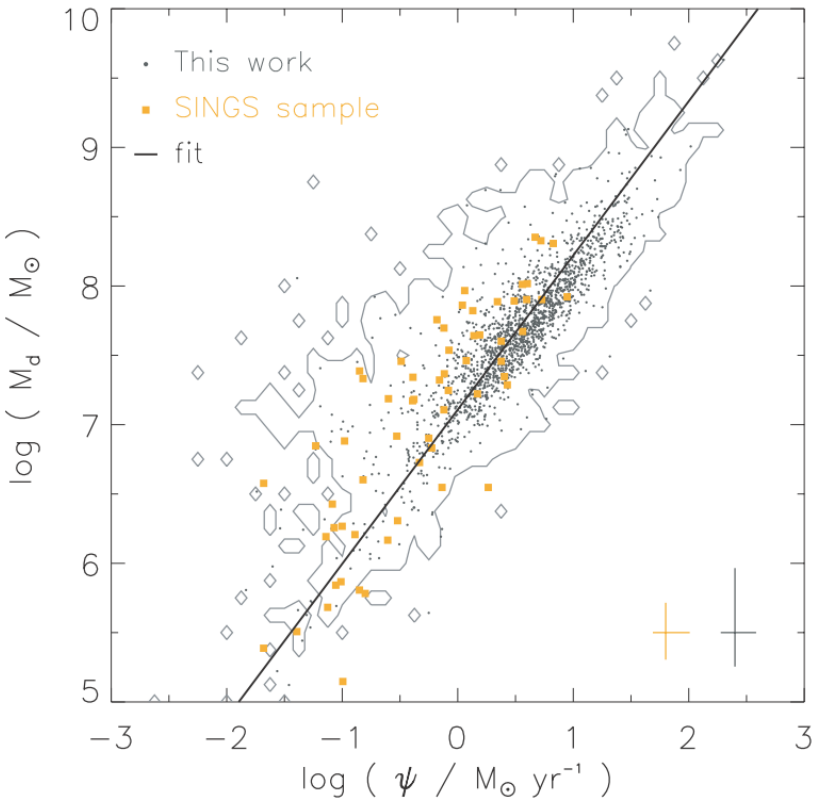

Fig. 6: Log-log scatter plot of dust mass and SFR estimates from (da Cunha et al., 2010). The yellow points serve only for a comparison to the SINGS survey's sample. The grey points indicate the estimates for the high-S/N subsample of da Cunha et al. while the grey contour shows the distribution of the full sample.

3.2 SFR and Dust Mass (da Cunha et al., 2010)

Elisabete da Cunha and Colleagues in 2010 published findings about the relation between star formation and dust in galaxies, particularly they report a formula for estimation of dust mass as a function of star formation rate. They, too, combine data sources, taking observations from SDSS and GALEX as well as the Infrared Astronomical Satellite (IRAS) and the Two Micron All Sky Survey. Their sample contains 3258 low-redshift galaxies, but they focus on a subsample 1658 sources with high S/N. The "assembly" of SPS modesl is done with code from (Bruzual and Charlot, 2003) and the estimation of galaxy properties is done quite analogously to (Salim et al., 2007), though da Cunha et al. use the median of the PDF rather than the mean as a final estimation.

Their most striking result is shown in Fig. 6: A tight correlation of SFR

(here denoted ψ) and galactic dust mass. The authors proceed to calculate fits of the two properties as functions of one another, the bisector of the resulting linear functions is the black line in Fig. 6. The function for it is reported as:

$$M_d = (1.28 \pm 0.02) \times 10^7 \, (\psi \, / \, M_\odot \mathrm{yr}^{-1})^{1.11 \pm 0.01} \, M_\odot \quad ,$$

where ψ again denotes the star formation rate. This empirical formula is a tool for estimation of one property by the other, with remarkably low uncertainties in the function's parameters. Judging roughly from the scatter plot (Fig. 6), it should be usable across regions of about 3 orders of magnitude in both quantities.

4 Results on Metallicity

Three publications will show the application of SPS on studying galaxies' metallicities in this section. From (Worthey, 1994), only the found degeneracy of galactic age and metallicity when using certain spectral features for SPS is mentioned. (Gallazzi et al., 2005) is treated in more detail, the examples then conclude with the smaller-scale study of (Thomas et al., 2003), which instead of the overall metallicity targets a single elemental abundance.

4.1 The Age-Metallicity Degenaracy (Worthey, 1994)

One well-known result concerning metallicity is a main outcome of a paper by Guy Worthey from 1994. He analyses SPS models of the time in detail, compares them with data and examines how galactic properties influence photometric indices, other features of the SED, and thus ultimately the outcome of estimations from modelling. Worthey finds that the effects on many of the typically utilised spectral features from an increase by a factor of 3 in the age of a stellar population and an increase in the population's metallicity by a factor of 2 are indistinguishable. Due to this *age-metallicity degeneracy*, SPS methods using these features cannot make valid statements about age or metallicity.

To solve this problem, Worthey identifies first features that do not suffer from the degeneracy, for instance Hβ and higher Balmer lines. The study illustrates the importance of the choice of features that comparisons between models and data are based on. The degeneracy is particularly problematic as ignoring it would not lead to a failure of the fitting procedure or obviously meaningless results, but rather to completely misleading estimates of age and metallicity.

4.2 Metallicity, Age and Stellar Mass in (Gallazzi et al., 2005)

A 2005 study by Anna Gallazzi and colleagues investigates metallicity alongside galactic age using SPS techniques, using a huge dataset (about 175 000 galaxies) from Data Release 2 of the SDSS. Their main results concern relations between the stellar mass content of galaxies and their metallcities and ages. They also go into detail about the limitations of the methods employed, discussing uncertainties and the feasible "resolution" of SPS parameter estimation, as well biases due to sample selection and inherent broad scatter in parameter distributions, the physical causes of which are simply not known yet.

4.2.1 Method

Gallazzi et al. apply the code provided by (Bruzual and Charlot, 2003) for their population synthesis. They are conscious of the age-metallicity degeneracy as well as the problem that calibration of the models is (necessarily) done on nearby stars, which renders several spectral features unsuitable as points of comparison to fit the data to. However, series of previous studies managed to identify absorption features that allow to produce reliable constraints from SPS on metallicity and age; Gallazzi et al. proceed to use the [Mg_2] and [MgFe]' features to constrain metallicity in their SPS fits, Hβ and the sum of Hδ_A and Hγ_A (Hδ_A+Hγ_A) to constrain age and include the D4000 spectral feature (a ratio of average fluxes in two bands around 4000 Å) for additional information about star formation rate.

With these five features selected, for a given combination of regarded galaxy and SPS model, the discrepancies between model and measurement are used to calculate a χ^2 and a weight $w = \exp(-\chi^2/2)$. Calculating these for 150000 plausible models per galaxy yields a probability density function for the parameters to be estimated. From the PDF the median is used as an estimator of the true galactic property, supplemented by formal errors calculated from the percentile range from 16 to 84 per cent (which corresponds to 1σ of a Gaussian distribution).

To check the validity of their method, the authors calculate the PDFs an additional time, using merely the age-sensitive indices for the fitting procedure. Furthermore, mock data with low S/N is created, fit the same way the real data is, and the resulting PDFs are examined. From all this two things are seen: First, age indeed is well-constrained by the age-sensitive indices alone, while metallicity PDFs deteriorate with the omission of their respective indices. Second, metallicity estimates are more sensitive to a lowering of

S/N. In the worst cases, their PDFs remain flat for multiples of the usual confidence intervals. That observation prompts Gallazzi et al. to exclude the low S/N part of their sample from final analyses, reducing the size to about 44000 galaxies. They continually check, however, how severely the sample reduction affects their results and report that no major systematic errors are induced. The boundary below which no meaningful estimation of metallicity can be derived is chosen at S/N = 20. For galactic age, on the other hand, no such sensitive S/N-dependence is reported.

4.2.2 Results

The most basic results of Gallazzi et al. are the median-likelihood estimates of the observed galaxies' metallicities, ages and stellar masses. Histograms of these are seen in Fig. 7 and already show for example that the most populated bins of the sample lie above Solar metallicity and that the typical stellar mass content of the observed galaxies lies within a range of 10^{10} to 10^{12} Solar masses.

Next to these simple histograms a more sophisticated analysis of the data is shown, the Hδ_A+Hγ_A vs D4000 diagrams: The galaxies are binned according to the strengths of the Hδ_A+Hγ_A and D4000 absorption features in their spectra, a bin width corresponding roughly to the measurement uncertainty. Now the bins are coloured in to indicate the average estimate of metallicity, age and mass within the bin.

A kind of broad diagonal sequence forms from the top left to the bottom right of the diagram. Previous studies (Kauffmann et al., 2003) have shown a relation between position in this diagram and star forming behaviour: Actively star forming galaxies tend to the top left while quiescent ellipticals dominate the bottom right. Also, for a fixed D4000 the strongest values of Hδ_A+Hγ_A have been associated with galaxies that experienced recent starbursts.

The results of Gallazzi et al. support the starburst findings: In the middle of the diagram's series, for most D4000 values the highest Hδ_A+Hγ_A bins also exhibit exceptionally high metallicity estimates. That finding is consistent with the hypothesis of recent metal-rich starbursts in the respective galaxies. Furthermore, general trends of increasing age as well as stellar mass towards the bottom right can be seen clearly.

The authors continue with an analysis of trends in metallicity and age as determined by stellar mass content. 8 summarises these results: At the top, doubly-logarithmic graphs show the added and re-normalised PDFs of the high-S/N subsample, split in 0.2 dex mass bins. A solid line traces the distributions' medians, while dashed lines indicate the regions from the 16th to the 84th percentiles. Both galactic properties appear to follow clear trends,

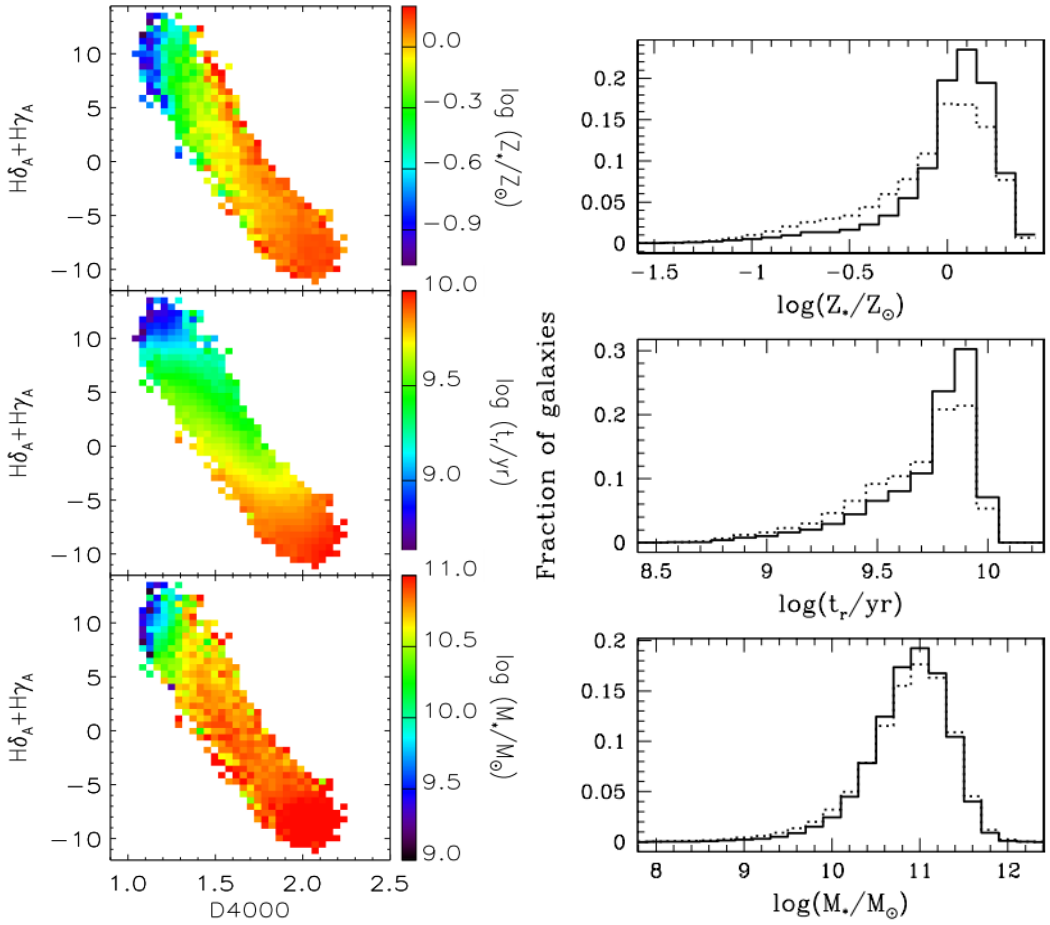

Fig. 7: Right: Basic results of the metallicity, age and stellar mass estimates in (Gallazzi et al., 2005). **Left:** Hδ_A+Hγ_A versus D4000 diagrams of the results

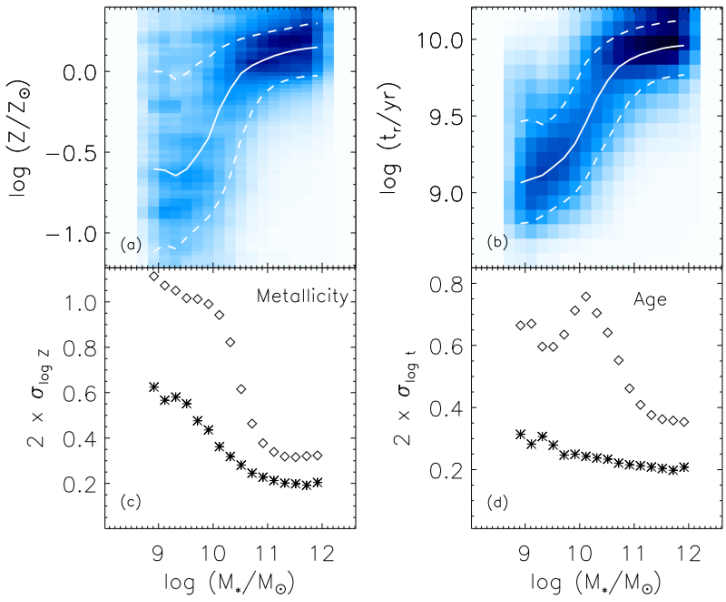

Fig. 8: Results from (Gallazzi et al., 2005), high S/N subsample, for metallicity and age as functions of galactic stellar mass. **Above:** PDFs combined into stellar mass bins and renormalised, solid lines trace medians, dashed lines 68 per cent confidence ranges. **Below:** Bin-by-bin comparison of confidence ranges (diamonds) to average formal errors (stars).

the medians increasing with greater stellar mass.

However, while the median trend in age is well constrained by its respective "corridor" of confidence intervals, the metallicity distributions exhibit a large scatter for lower stellar mass content. This scatter might be inherent to the sample, or it might just be a consequence of large uncertainty in parameter estimation at lower stellar mass content. To decide between these alternatives, the 68 per cent confidence ranges of the distributions are compared, bin by bin, with the average formal errors of the parameter estimation. Those comparisons are seen in the bottom graphs: there is an increase in uncertainty for the metallicities at lower stellar mass content, but this cannot explain the full scatter. Especially at intermediate stellar mass content, more so even for the galactic ages, distribution scatter exceeds the average uncertainty. Thus, despite clear trends, metallicity and age are certainly not uniquely determined by stellar mass content.

4.3 An investigation of Calcium underabundance (Thomas et al., 2003)

SPS studies on metallicity are done on a smaller scale as well. In 2003, D. Thomas, C. Maraston and R. Bender used models they developed them-

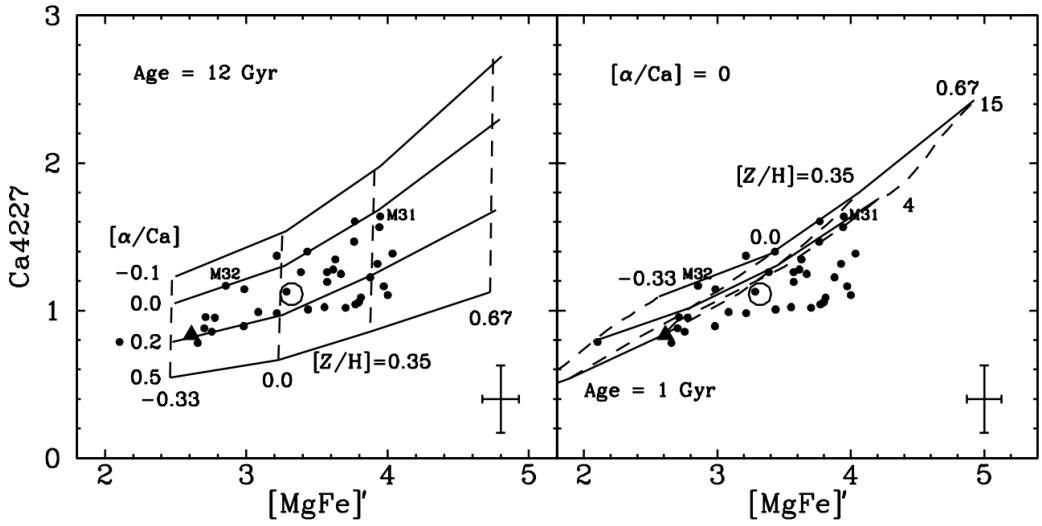

Fig. 9: Measurements of Ca4227 vs [MgFe]' used in (Thomas et al., 2003). The open circle indicates the sample's median, the triangle bulge light of the Milky Way. Lines correspond to modelling as discussed in the text.

selves and published the same year, and with those investigated the Ca4227 absorption-line feature in the spectra of elliptical galaxies. The models were calibrated on globular cluster data. At the time, only one data set was available that contained the desired Calcium line for ellipticals, limiting the sample to 39 galaxies.

Calcium is an alpha element (its most abundant isotope's mass number being a multiple of four), but is known in elliptical galaxies to be less abundant than other alpha elements. In particular, the authors talk of "Calcium underabundance" when the ratio α/Ca, abundance of other alpha elements over that of Calcium, is larger than solar, and thus $[\alpha/\mathrm{Ca}] > 0$, with

$$[\alpha/\mathrm{Ca}] := \log\left(\frac{X_\alpha}{X_{\mathrm{Ca}}}\right) - \log\left(\frac{X_\alpha}{X_{\mathrm{Ca}}}\right)_\odot = \log\left(\frac{X_\alpha/X_{\mathrm{Ca}}}{X_{\alpha\odot}/X_{\mathrm{Ca}\odot}}\right) \quad ,$$

where the Xs denote the respective abundances.

The authors attempt to fit age and metallicity to the observed Ca4227, but their models do not reproduce observational findings, as is seen in 9. There, Ca4227 is plotted against the [MgFe]' spectral feature, which serves as an indicator of general metallicity. The solid and dashed lines represent the combinations of the two features as predicted by various models, for constant age in the left graph, for constant α/Ca in the right. Especially the right one shows how a sizable fraction of the sample resides at lower α/Ca than any model displayed, the authors report that none of the models predict suitably

low α/Ca. It is therefore concluded that elliptical galaxies are systematically underabundant in Calcium, compared to SPS modelling of the time.

5 Discussion

The basic idea of SPS is quite versatile and allows for many kinds of implementations, with different indicators in the SED getting used, different assumptions about star formation history, chemical composition, dust properties et cetera; and the fitting procedure adds freedom as well. On the flip side, this richness of possibilities makes any results from SPS strongly model dependent. Great care is required to validate procedures against each other, and it is not surprising in this context that authors tend to rely on approaches that appear oversimplified at first glance (e.g. a single metallicity for all star formation of a galaxy).

A typical criticism levelled against fitting of complicated data concerns large numbers of fitting parameters. The problem is that, especially when the number of data points is not comparatively large, a function with many parameters can be fit to any sort of data without a meaningful interpretation. This problem, surprisingly, does not occur with typical SPS routines. In fact, single parameter χ^2 minimising is a standard approach among these methods – the actual galactic properties not being fitting parameters. The downside of this is the requirement of huge libraries of models to compare the data to.

Phenomena like the age-metallicity degeneracy reveal another problem that is not specific to the SPS technique, but rather stems from the strictly observational nature of astronomy itself. In many cases, more than one possible cause to the phenomena observed exists; and no experiments can be carried out that would show characteristics obtained from a carefully set up single "cause". Results from multiple observational techniques must be taken into account to become more confident about the validity of deductions.

For instance, Salim et al. identified their groups of galaxies with and without star formation or AGN with tools beyond their standard fitting routine. In that way, they took care to make the classification independent from their galactic property estimations. On the other hand, though, AGN are still poorly understood, so it is not unthinkable that they might have effects on the SED that influence the estimation of star formation rate.

In general, in the study of galaxies beyond the Milky Way and its nearest neighbours, simulations seem an indispensable tool if results are supposed to transcend rough shapes and rotation curves. However, pitfalls of physical modelling abound and it is imperative to be aware be aware of and take precautions against as many of these as possible. In particular, no single

method should be trusted completely. In this way, the modifiability of the SPS approach provides an advantage to the technique. The example stuides in this review successfully employ SPS to estimate galactic properties and validate their results against other methods. They provide starting points for discussion about the behaviour of objects that are so far poorly understood, as in the example of a "star forming sequence" bridged by AGN-hosting galaxies in (Salim et al., 2007) or the systematic Ca underabundance not explainable by models in (Thomas et al., 2003).

References

Bruzual, G. and Charlot, S.: 2003, MNRAS **344**, 1000

Conroy, C.: 2013, *Annual Review of Astronomy and Astrophysics* **51**, 393

da Cunha, E., Eminian, C., Charlot, S., and Blaizot, J.: 2010, MNRAS **403**, 1894

Gallazzi, A., Charlot, S., Brinchmann, J., White, S. D. M., and Tremonti, C. A.: 2005, MNRAS **362**, 41

Kauffmann, G., Heckman, T. M., White, S. D. M., Charlot, S., Tremonti, C., Brinchmann, J., Bruzual, G., Peng, E. W., Seibert, M., Bernardi, M., Blanton, M., Brinkmann, J., Castander, F., Csábai, I., Fukugita, M., Ivezic, Z., Munn, J. A., Nichol, R. C., Padmanabhan, N., Thakar, A. R., Weinberg, D. H., and York, D.: 2003, MNRAS **341**, 33

Salim, S., Rich, R. M., Charlot, S., Brinchmann, J., Johnson, B. D., Schiminovich, D., Seibert, M., Mallery, R., Heckman, T. M., Forster, K., Friedman, P. G., Martin, D. C., Morrissey, P., Neff, S. G., Small, T., Wyder, T. K., Bianchi, L., Donas, J., Lee, Y.-W., Madore, B. F., Milliard, B., Szalay, A. S., Welsh, B. Y., and Yi, S. K.: 2007, *The Astrophysical Journal Supplement Series* **173**, 267

Thomas, D., Maraston, C., and Bender, R.: 2003, MNRAS **343**, 279

Worthey, G.: 1994, *The Astrophysical Journal Supplement Series* **95**, 107